

Intracluster light and the extended stellar envelopes of cD galaxies: An analytical description

Marc S. Seigar^{1*†}, Alister W. Graham² and Helmut Jerjen³

¹Center for Cosmology, Department of Physics & Astronomy, University of California, Irvine, 4129 Frederick Reines Hall, Irvine, CA 92697-4575, USA

²Centre for Astrophysics & Supercomputing, Swinburne University of Technology, Hawthorn, Victoria 3122, Australia

³Research School of Astronomy & Astrophysics, Mount Stromlo Observatory, Cotter Road, Weston Creek, ACT 2611, Australia

In original form 19 October 2006

ABSTRACT

We have analysed deep R -band images, down to a limiting surface brightness of $26.5 R\text{-mag arcsec}^{-2}$ (equivalent to $\sim 28 B\text{-mag arcsec}^{-2}$), of 5 cD galaxies to determine the shape of the surface brightness profiles of their extended stellar envelopes. Both de Vaucouleurs $R^{1/4}$ model and Sérsic’s $R^{1/n}$ model, on their own, provide a poor description of the surface brightness profiles of cD galaxies. This is due to the presence of outer stellar envelopes, thought to have accumulated over the merger history of the central cluster galaxy and also from the tidal stripping of galaxies at larger cluster radii. We therefore simultaneously fit two Sérsic functions to measure the shape of the inner and outer components of the cD galaxies. We show that, for 3 out of our 5 galaxies, the surface brightness profiles are best fit by an inner Sérsic model, with indices $n \sim 1 - 6$, and an outer *exponential* component. For these systems, the galaxy-to-envelope size ratio is $0.1 - 0.4$ and the contribution of the stellar envelope to the total R -band light (i.e. galaxy + envelope) is around 60 to 80 per cent (based on extrapolation to a 300 kpc radius). The exceptions are NGC 6173, for which our surface brightness profile modelling is consistent with just a single component (i.e. no envelope) and NGC 4874 which appears to have an envelope with a de Vaucouleurs, rather than exponential, profile.

Key words: galaxies: elliptical and lenticular, cD – galaxies: formation – galaxies: fundamental parameters – galaxies: haloes – galaxies: structure

1 INTRODUCTION

First-ranked galaxies in clusters, also referred to as brightest cluster galaxies (BCGs), are the brightest and most massive galaxies in the Universe. They are typically elliptical galaxies (Lauer & Postman 1992). About 20% of BCGs appear to be surrounded by a large, low surface brightness envelope and are additionally referred to as cD galaxies (e.g. Dressler 1984; Oegerle & Hill 2001). Such cDs reside only in clusters and groups, never in the field. Their existence and evolution are intimately tied to the formation and evolution of the clusters themselves. The detection of these envelopes, however, is somewhat problematic.

For a time, every elliptical galaxy was thought to have a stellar distribution whose projection on the plane of the

sky was described by de Vaucouleurs (1948) $R^{1/4}$ law. This is reflected by the status of "law" that is ascribed to what is a highly useful, but nonetheless empirical "model". However, Lugger (1984) and Schombert (1986) have shown that all luminous, elliptical galaxies, including brightest cluster galaxies, have excess flux at large radii relative to their best-fitting $R^{1/4}$ models. Moreover, today, it is known that only elliptical galaxies with $M_B \sim -20.5$ mag have $R^{1/4}$ profiles (e.g. Kormendy & Djorgovski 1989). Brighter and fainter elliptical galaxies are better described by Sérsic’s (1963) $R^{1/n}$ model (see Graham & Driver 2005 for a review) with the index n taking on values that are greater and smaller than 4, respectively (e.g. Caon, Capaccioli & D’Onofrio 1993; Young & Currie 1994; Graham et al. 1996; Graham & Guzmán 2003, and references therein). This then leads to the question as to whether the excess flux observed in cD galaxies (e.g. Feldmeier et al. 2002; Liu et al. 2005) is due to a distinct and separate halo of material, or is instead a manifestation

* E-mail: mseigar@uci.edu (MSS)

† McCue Fellow

Table 1. Column 1: galaxy name. Column 2: host cluster name. Column 3: richness class from the catalogue of Abell (1958). Column 4: Type from Bautz & Morgan (1970). Column 5: galaxy redshift taken from the NASA/IPAC Extragalactic Database (NED). Column 6: physical scale, i.e. the distance in kpc that is equivalent to an angular distance of $1''$, calculated using a Hubble constant, $H_0 = 70 \text{ km s}^{-1} \text{ Mpc}^{-1}$. Columns 7 and 8: right ascension and declination of the galaxy. Columns 9 and 10: right ascension and declination of the nearby blank field. Column 11: worst seeing of each galaxy image. Column 12: radial extent of the data.

Galaxy	Cluster	R.C.	BM Type	z	Scale (kpc/'')	RA (J2000) Galaxy	Dec (J2000)	RA (J2000) Blank field	Dec (J2000)	Seeing (arcsec)	Extent of data (kpc)
1	2	3	4	5	6	7	8	9	10	11	12
GIN 478	Abell 2148	0	–	0.090	1.73	16:01:13.9	+25:27:13	16:13:15.4	+25:28:43	~1.2	223
NGC 3551	Abell 1177	0	I	0.032	0.62	11:09:44.4	+21:45:32	10:57:40.2	+21:47:01	~1.3	102
NGC 4874	Abell 1656	2	II	0.024	0.47	12:59:35.7	+27:57:34	12:56:30.9	+27:53:45	~1.5	61
NGC 6173	Abell 2197	0	II-III	0.029	0.57	16:29:44.9	+40:48:42	16:41:52.3	+40:47:53	~2.2	94
UGC 9799	Abell 2052	0	I-II	0.034	0.67	15:16:44.5	+07:01:17	15:28:20.5	+07:00:53	~2.4	96

from the application of, or at least comparison with, an inappropriate fitting function, namely the $R^{1/4}$ model.

To address this question, and to derive both the size and flux ratio of any possible outer envelope relative to the inner galaxy component, obviously one should not apply the $R^{1/4}$ model to the inner light-profile. It would similarly be a mistake to simply fit an $R^{1/4}$ model to any suspected outer halo. We have therefore set out to *measure* the shape of the projected stellar distribution through the simultaneous application of two $R^{1/n}$ models to the light-profiles from deep exposures of galaxies reported to be cD galaxies.

In this paper we analyse *R*-band images for 5 cD galaxies observed to a depth of $\mu_R = 26.5 \text{ mag arcsec}^{-2}$, at the 3σ level, with the main purpose of determining the shapes of the surface brightness profiles of their low surface brightness stellar envelopes. From this we also determine the galaxy-to-envelope size ratios and the envelope-to-total flux ratios within 300 kpc, and also when applying no outer truncation to the best fitting models¹. These parameters can then be used to constrain models of cD galaxy, and host cluster, formation. This paper is arranged as follows. Section 2 describes our observations and data reduction, including the ellipse fitting and surface brightness profile fitting method; Section 3 presents the results of the surface brightness profile fitting and discusses the best fit in each case. In Section 4 we provide a brief review on the formation process of BCGs and then go on to discuss our findings. Finally, in Section 5 we summarise our main results.

2 OBSERVATIONS AND DATA REDUCTION

2.1 Data

The light profiles presented in this paper are derived from broad *R*-band images of 5 cD galaxies observed to a depth of $\mu_R = 26.5 \text{ mag arcsec}^{-2}$ at the 3σ level. For elliptical galaxies, Worthey (1994) reports that $B - R = 1.65$ and Lauer & Postman (1994) find $B - R = 1.51$, and so our surface brightness limit is equivalent to a *B*-band depth of $\simeq 28 \text{ mag arcsec}^{-2}$. This is $\sim 3 \text{ mag arcsec}^{-2}$ deeper than the study of BCGs presented by Graham et al. (1996). Our

galaxy sample was selected from two samples of BCGs: one observed by Lauer & Postman (1994), the other by Hill & Oegerle (1993). The selection criteria for these galaxies was that they (i) were classified as cD galaxies, (ii) had a limiting redshift $z < 0.1$, and (iii) were visible from La Palma in late April. Of the galaxies that met the selection criteria, we observed five; they are listed in Table 1.

On each night at least four standard stars from the Landolt (1992) list were observed, at varying airmass, in order to determine the photometric zero-point and the airmass extinction correction for the data. These have been applied to each image. Corrections for surface brightness dimming, galactic extinction and K-correction have also been applied. Throughout this paper, magnitudes are quoted using the Vega system.

For each galaxy, one nearby blank field (see Table 1) was also observed for the purpose of estimating the sky-background free from any intracluster light. The observations were taken in such a way that the object frames and sky frames were interleaved. The observations were made during dark time with the 1.0-m Jacobus Kapteyn Telescope (JKT) on the island of La Palma. These observations were taken on the nights of 2003 April 24–30 using the 2048×2048 SITe2 CCD camera, which has 0.331 arcsec pixels and a field-of-view $11.3 \times 11.3 \text{ arcmin}^2$. The filter used was a standard Harris *R* band filter. The observations of both the galaxy fields and the blank fields consisted of 24 co-added exposures of 900 seconds. The exceptions to this are NGC 3551 and NGC 4874, where only 12 co-added exposures were made due to bad weather.

Data reduction was performed within IRAF. All images were bias-subtracted, and then flat fielded using twilight flats. Images were then combined by degrading the best images, by convolution with a Gaussian, to match the seeing conditions in the worst image, which was typically $\sim 1'' - 2''$ (see Table 1). There was no evidence for any fringing effects in any of the images. The blank sky images were then used to estimate the sky-background and these values were subtracted from the galaxy images. In performing the sky-background estimation, ten areas of the blank sky image were used to calculate 10 medians. The sky value was then taken as the mean of these 10 medians, and the average deviation was adopted as the uncertainty in the sky background.

Uncertainties in the estimation of the sky-background are the dominant source of error in determining the shape of

¹ The radial extent of our data is typically $\sim 100 \text{ kpc}$, and so we have to extrapolate to the truncation radius.

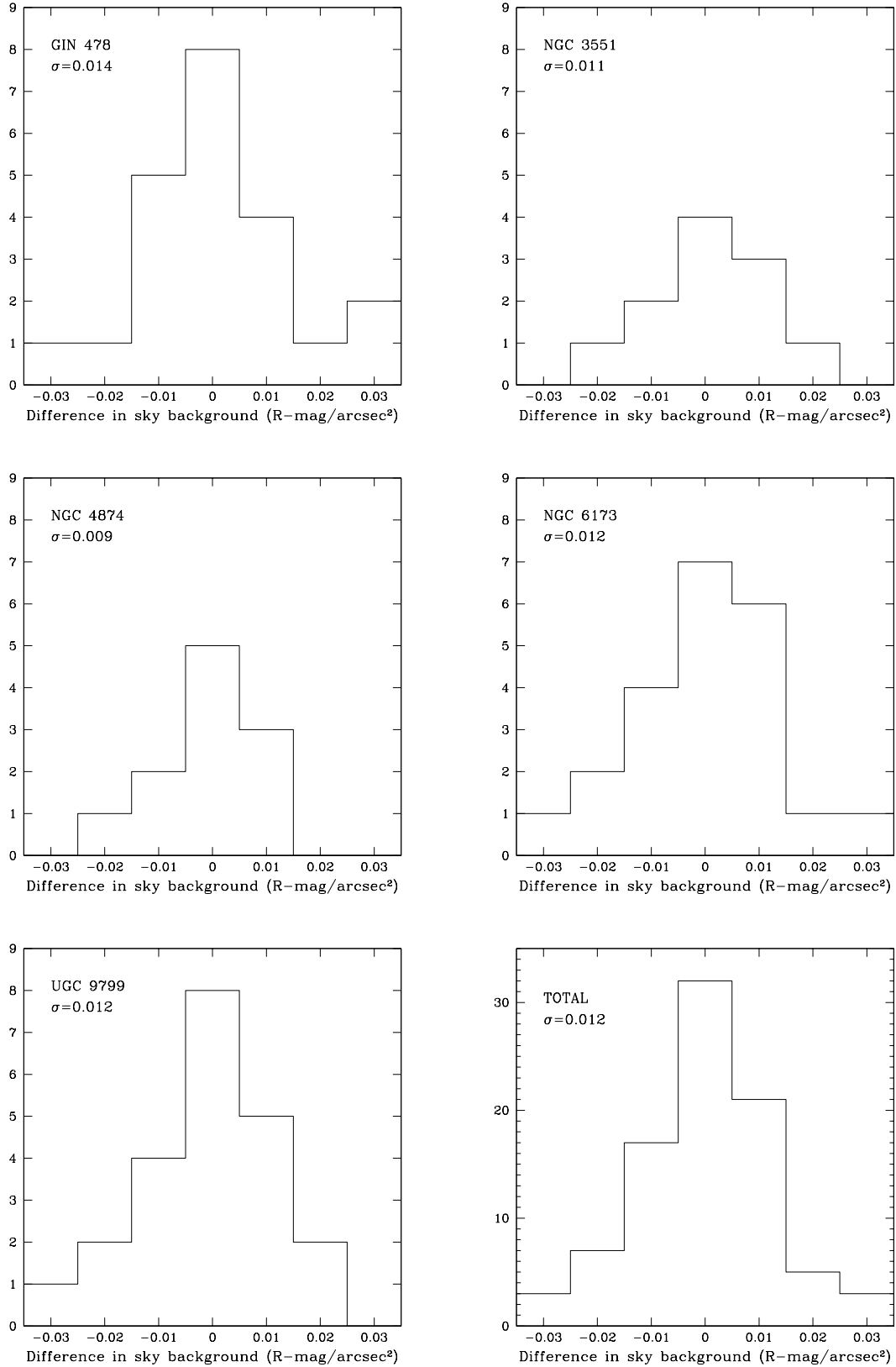


Figure 1. Differences in the sky background, δ_i , obtained from consecutive sky frames near each galaxy, and for the total dataset (bottom right panel). Each panel shows the associated sample standard deviation $\sigma = \sqrt{\sum_i^n \delta_i^2 / (n - 1)}$, where n is 11, 22 or 88 depending on the panel.

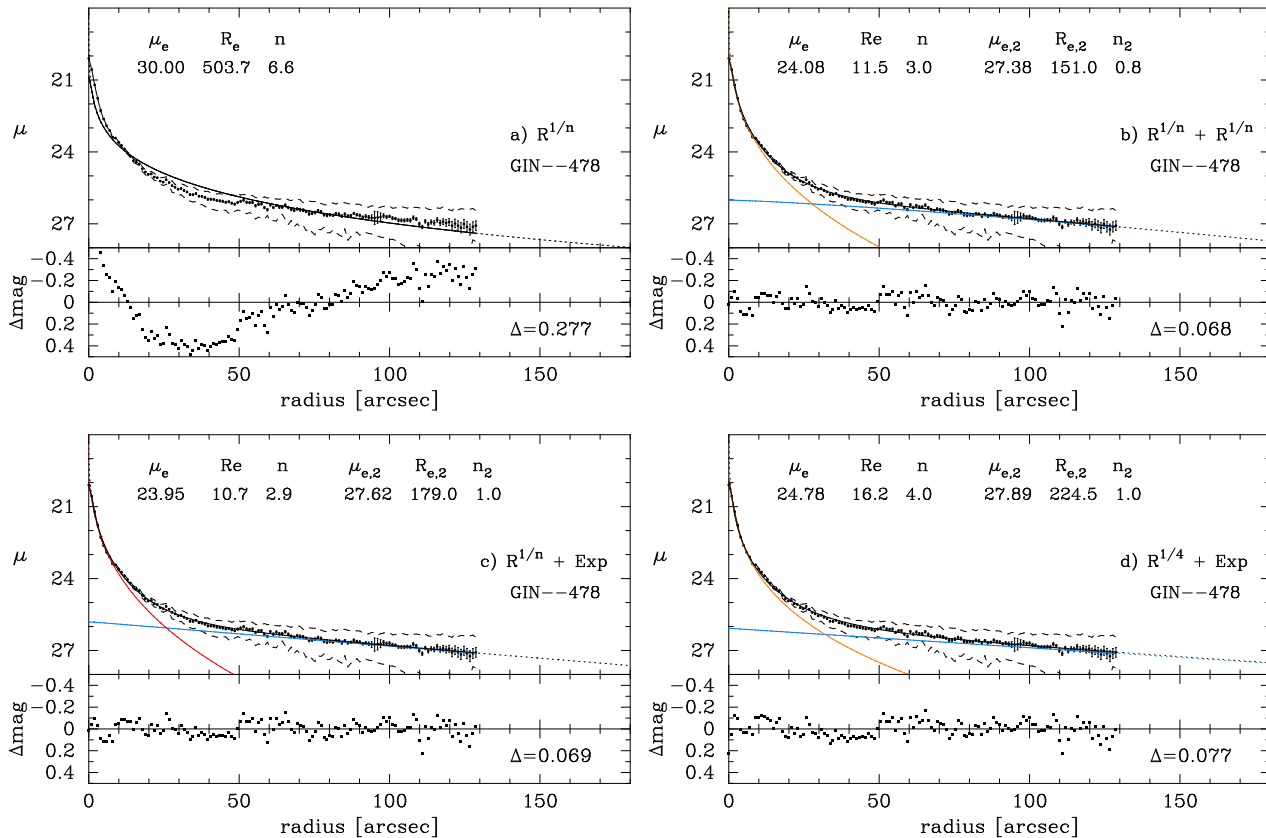


Figure 3. Surface brightness profile for GIN 478 with different analytic fits: (a) Sérsic model; (b) double Sérsic model; (c) Sérsic + exponential model; (d) $R^{1/4}$ + exponential model. Open circles at small radii are excluded from the fits. The root mean square (rms) scatter, Δ , is shown in the lower portion of each figure. The dashed lines indicate the extracted surface brightness profile with the sky uncertainty added and subtracted. We note that an arbitrary upper limit of $\mu_e = 30 \text{ mag arcsec}^{-2}$ in our software is reached in panel (a), reflecting the inadequacy of a single $R^{1/n}$ function to describe the observed stellar distribution.

the outer part of the galaxy surface brightness profiles. The above estimates of this error have been used in Section 2.3 to quantify the variation in the optimal parameters of the fitted models. Here we adopt an alternative approach to gauge the size of this error. Because of the way we interlaced our target and sky frames, the sky-background in each such pair of observations may differ. In Figure 1 we show histograms of the difference in the sky background between consecutive sky frames for each galaxy. Each offset in these histograms roughly represents twice the expected background offset between an individual target and sky frame, for which only half as much time has elapsed between their acquisition. As can be seen, the median value for this difference is consistent with the sky frames having similar values for the background. The sample standard deviation, σ , is only $\sim 0.012 \text{ mag arcsec}^{-2}$. A dominant monotonic drift in the background as one progresses through the night would produce a non-zero median value in the distributions to either positive or negative values. Given N ($=11$ or 22) pairs of sky frames, the expected difference in the final sky-background level of each is given by σ/\sqrt{N} . This amounts to 0.0026 – $0.0036 \text{ mag arcsec}^{-2}$ uncertainty, consistent with the sky errors calculated using the method above.

2.2 Extraction of surface brightness profiles

We have employed and compared two methods for the extraction of the surface brightness profiles from the galaxy images.

The first is isophotal ellipse fitting, performed using the **Ellipse** routine in **IRAF** which uses an iterative method described by Jedrzejewski (1987). Each isophote was fitted allowing for a variable position angle and ellipticity, but holding the centre fixed. Foreground and background sources were masked out within the **Ellipse** routine. Given our interest in the outer light-profile, we chose to sample the surface brightness profile using a standard, albeit somewhat arbitrary, linear spacing. A logarithmic spacing would have generated a lot of data points, and hence more weight, at small radii. The **Ellipse** routine works in such a way, that ellipses are set up centered on the central cD galaxy. This defines several elliptical annuli. The surface brightness at each annulus is calculated as the average number of counts within that annulus. The uncertainty on the surface brightness is calculated as the rms between pixels divided by $\sqrt{N-1}$, where N is the number of pixels. The statistical error is therefore dependent upon the step size between annuli or ellipses. However, at large radii, the actual error on the computed surface brightness, is dominated by uncertainty in the sky background, and we discuss this later.

The second method that we used determines the sur-

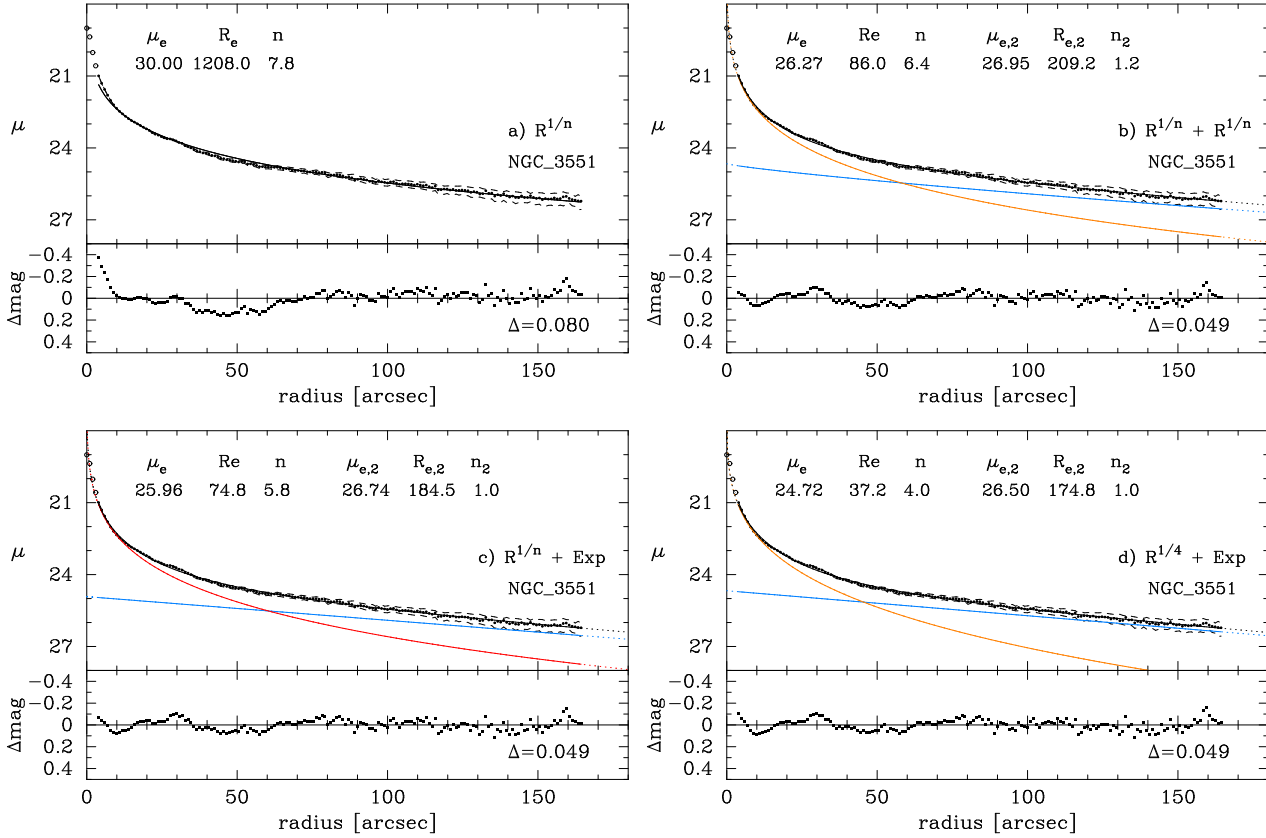


Figure 4. Same as Figure 3, but for NGC 3551.

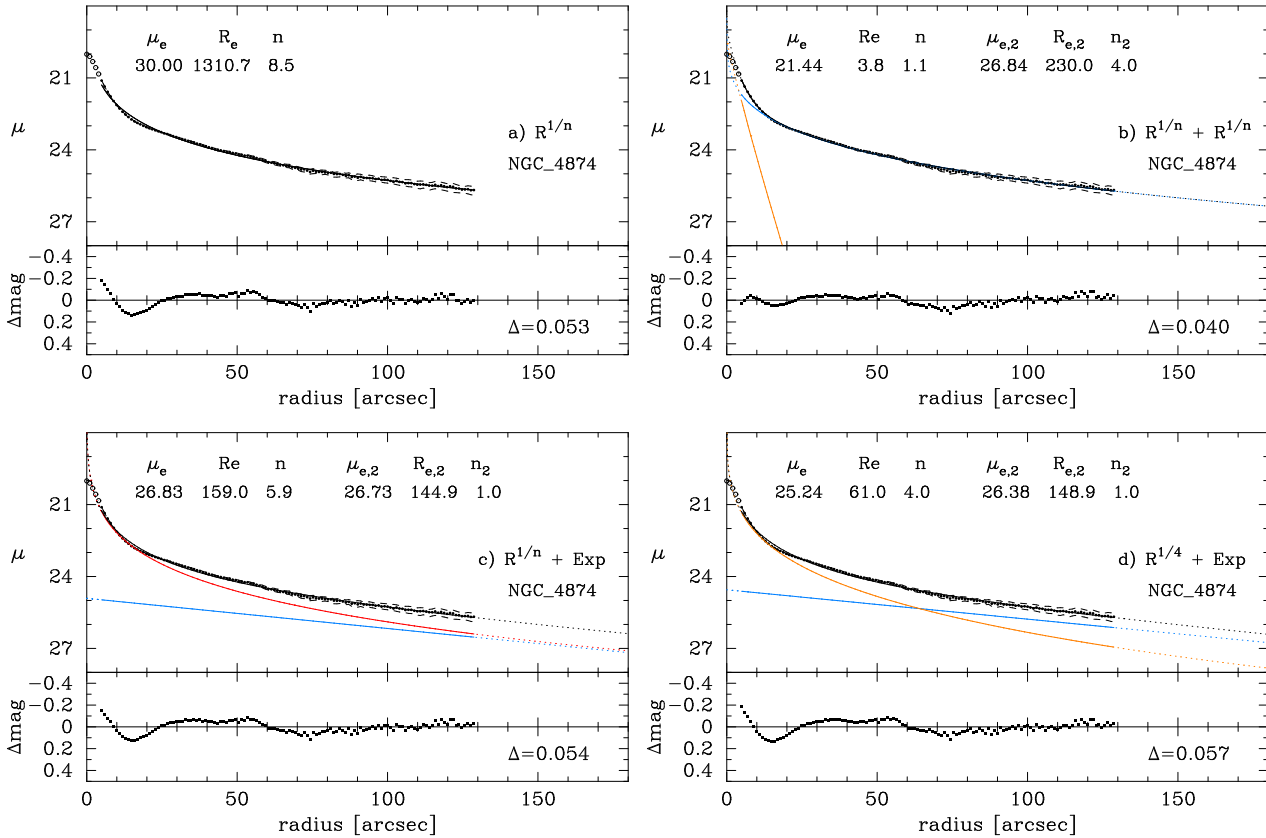


Figure 5. Same as Figure 3, but for NGC 4874.

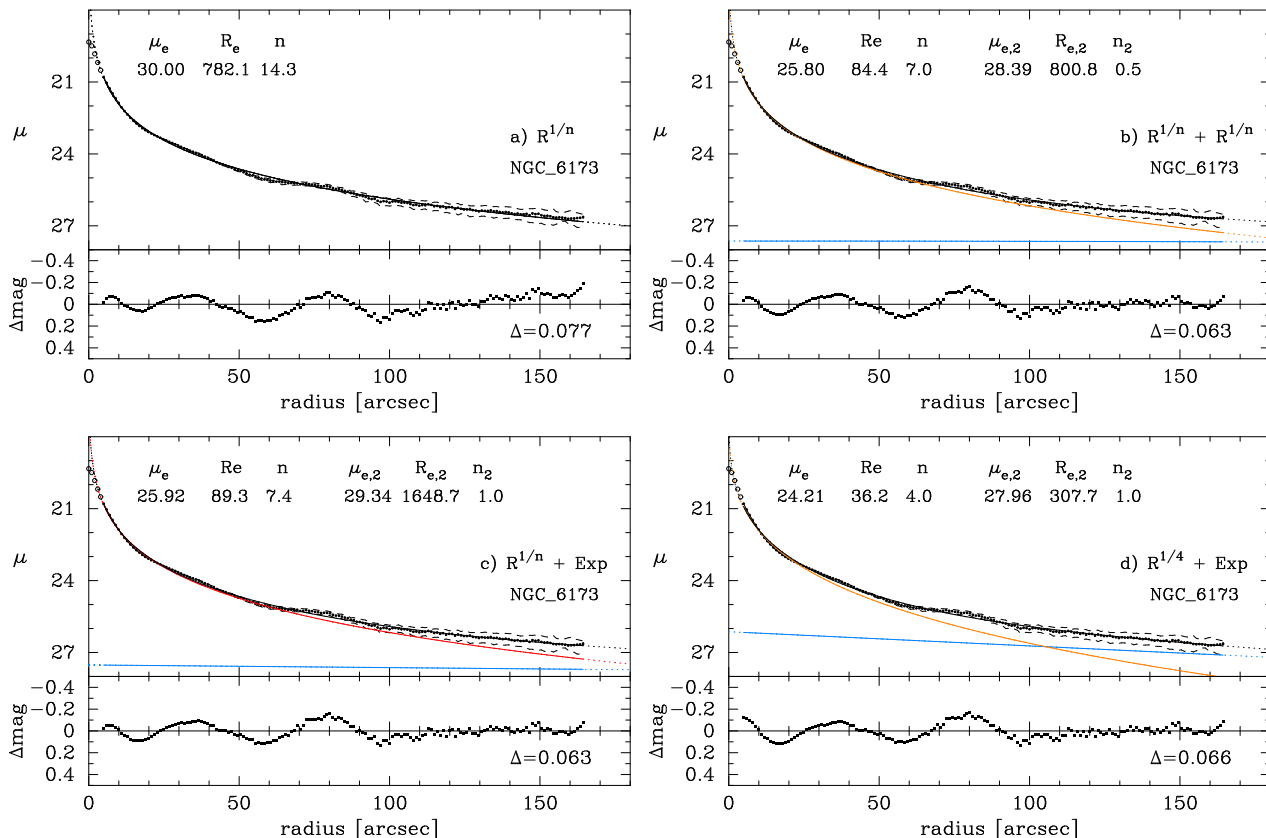


Figure 6. Same as Figure 3, but for NGC 6173. The high value of $R_{e,2}$ in panel (b) is not a software limit. It is instead an indication that we may be merely fitting an inadequately subtracted sky-background with the outer $R^{1/n}$ function.

face brightness profiles with the help of another isophotal fitting routine also written in **IRAF** (Jerjen, Kalnajs & Bingeli 2000; Barazza, Bingeli & Jerjen 2002). After foreground stars and neighbouring galaxies were removed from the image, a symmetrical 2-D model was reconstructed from the observed light distribution allowing isophotal ellipticity and position angle to vary with radius, but keeping the luminosity-weighted centre fixed. This fitting process was repeated iteratively until the residuals were minimised. The 1-D surface brightness profiles were then calculated from the 2-D model by adopting mean values for ellipticity and position angles.

Figure 2 shows the reduced images (left panel) and the residual images (right panel) of the 5 cD galaxies in our sample. The residual images were produced by subtracting an azimuthally symmetrical model from the original data.

Both sets of surface brightness profiles, and the subsequent modeling, generated consistent results. From here on we refer to only the surface brightness profiles extracted using the **IRAF** task, **Ellipse**, presented in Figures 3 to 7. The dashed lines in Figures 3 to 7 represent the extracted surface brightness profile after adding (upper dashed line) and subtracting (lower dashed line) the uncertainty in the sky background. Note that this uncertainty was added to or subtracted from the image, and then the new surface brightness profile was derived. Because this uncertainty is applied to the image, the dashed lines sometimes do not necessarily fall either side of the data points. This is because it is possible for the **Ellipse** routine to fit the image with slightly

different ellipticities and position angles, and so a small adjustment in the surface brightness results.

2.3 Modelling the surface brightness profiles

Our modelling of the surface brightness profiles employs the Sérsic (1963, 1968) model for both the inner part of the galaxy and the outer stellar envelope.

The Sérsic $R^{1/n}$ radial intensity profile can be written as

$$I(R) = I_e \exp \left\{ -b_n \left[\left(\frac{R}{R_e} \right)^{1/n} - 1 \right] \right\}, \quad (1)$$

where I_e is the intensity at the effective radius, R_e , which encloses 50 per cent of the light. The factor b_n is a function of the shape parameter, n , such that $\Gamma(2n) = 2\gamma(2n, b_n)$, where Γ is the gamma function and γ is the incomplete gamma function (see Graham & Driver 2005). In the case where $n = 1$, the Sérsic model is equivalent to an exponential, and when $n = 4$ it is equivalent to the $R^{1/4}$ model.

Initially, for all the galaxies, we attempt to fit the entire surface brightness profile with a single Sérsic component. We also test the applicability of fitting an inner $R^{1/n}$ model and an exponential model to the outer envelope (i.e., in a similar way to the case for disk galaxies, e.g., Andredakis et al. 1995; Seigar & James 1998; Graham 2001). We then go on to use a multitude of fits (not all shown), which keep the inner and outer Sérsic indices fixed at integer values between 1 and 4. Finally, we allow both of the Sérsic indices to vary.

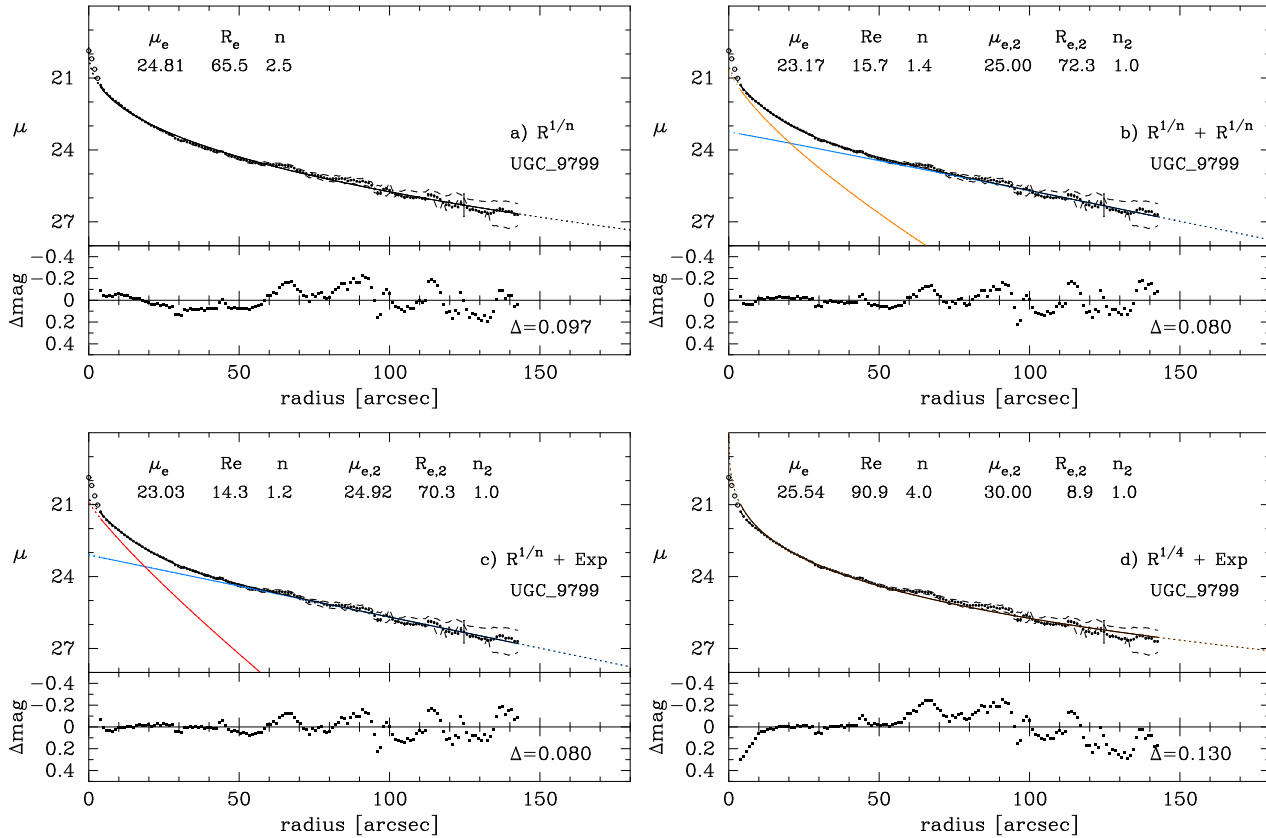


Figure 7. Same as Figure 3, but for UGC 9799. In panel (d), the outer exponential component does not contribute to the fit, and is thus not seen. The excess central flux seen in panels (b) and (c) are from the AGN.

Corrections for the effects of seeing have been made using the prescription given in Pritchett & Kline (1981). Due to the Gaussian nature of the JKT point spread function (psf) it is not necessary to consider more complicated seeing corrections. For any intrinsically radially symmetric intensity distribution, $I(R)$, the observed seeing-convolved profile, $I_c(R)$, is

$$I_c(R) = \sigma^{-2} e^{-R^2/2\sigma^2} \int_0^\infty I(x) I_0(xR/\sigma^2) e^{-x^2/2\sigma^2} x dx, \quad (2)$$

where σ is the dispersion of the Gaussian psf, which is equal to the full-width half maximum (FWHM) divided by a factor of 2.3548. The I_0 term is the zeroth-order modified Bessel function of the first kind (e.g. Press et al. 1986). This approach to correcting light profile shapes for seeing was adopted by Andredakis, Peletier & Balcells (1995) and later by de Jong (1996).

Due to the potential presence of partially depleted cores in luminous elliptical galaxies (e.g., Lauer et al. 1995; Graham et al. 2003; Trujillo et al. 2004; Ferrarese et al. 2006 and references therein), or instead the presence of multiple nuclei from semi-digested mergers, the innermost seeing-effected data points ($\sim 3''$, $\sim 2-5$ kpc) have been excluded from the fits. In comparison, the inner 10-20 kpc were excluded from the BCG analysis in Zibetti et al. (2005), where the FWHM was ~ 5 kpc. It is because of such features that one should not model integrated aperture magnitude profiles, in which every data point is effected/biased. Instead, one should fit the surface brightness profiles directly. Because of the AGN

in UGC 9799, the inner 4 data points were excluded. Obviously, given that we have excluded the most seeing affected data, the use of equation 2 to convolve our $R^{1/n}$ models before fitting them to the observed light profiles is not so crucial. Deactivating the seeing correction has no significant affect.

The best-fitting models were acquired using the subroutine UNCMND from Kahaner, Moler & Nash (1989). At each iteration, the nonlinear Sérsic functions are approximated by a quadratic function derived from a Taylor series. The quadratic function is minimised to obtain a search direction, and an approximate minimum of the nonlinear function along the search direction is found using a line search. The algorithm computes an approximation to the second derivative matrix of the nonlinear function using quasi-Newton techniques.

Common practice when fitting a model to some data set is to employ the use of the χ^2 statistic, such that the reduced- χ^2 is given by,

$$\chi^2 = \frac{\sum_{i=1}^m \delta_i^2 / \sigma_i}{m - k}, \quad (3)$$

where m is the number of data points, δ_i is the i th residual (about the best-fitting model), σ_i is the uncertainty on the i th data point and k is the number of parameters in the fitted model.

Such an approach is highly desirable *if* one knows what the functional form of the underlying model is. However, when one does not know the form of the underlying model,

but instead has to assume some empirical function such as de Vaucouleurs model or Sérsic's model, the use of the reduced- χ^2 statistic can produce rather biased results. For example, at the centre of a galaxy, the signal-to-noise ratio is high, and thus the uncertainties (σ_i) that are assigned to the central data are small. These points thus have considerable weight in determining the best fit, obtained by minimising the reduced- χ^2 value. In the past, the reduced- χ^2 statistic has been used to fit Sérsic bulges plus exponential disks to spiral galaxy light profiles. However, due to the presence of additional (un-modelled) nuclear components, the bulge model and the simultaneously-fit disk model have been heavily biased (see Balcells et al. 2003). That is, because the assumed model (bulge + disk) did not match the true underlying distribution (bulge + a disk + an additional nuclear component), the small uncertainties on the data at small radii heavily biased the fits to produce erroneous results (see e.g., Schombert & Bothun 1987).

We do not know the structural make-up of our 5 cD galaxies, they may contain a third component, such as a bar or a lens or indeed multiple nuclear components that we do not model. We therefore wish to avoid use of the χ^2 statistic.

Furthermore, another main concern is that we wish to quantify the stellar distribution of the suspected outer envelope. In using equation 3, the (signal-to-noise)-weighted values of σ_i will act to erase the value or worth of the data at large radii. Moreover, in trying to gauge the influence of sky-background errors, likely to be a major source of uncertainty on the shape of the outer stellar distribution, the use of equation 3 would dilute the effect of adding and subtracting the uncertainty in the sky-background, and give one the false belief that their fitted models have less variance than they really ought. This is because correlated errors are not taken into account when computing the χ^2 value.

A common approach, which circumvents the above two problems, and which we have adopted, is to use the root mean square (rms) scatter

$$\Delta = \sqrt{\frac{\sum_{i=1}^m \delta_i^2}{m}}. \quad (4)$$

The results of our profile fitting are shown in Figures 3–7. The Sérsic indices, effective radii and effective surface brightnesses are listed in Table 2. Uncertainties on the best-fitting parameters (Table 2) are obtained by repeating the fit to the surface brightness profiles after adding and subtracting the 1σ uncertainty in the sky-background level. It should be noted that the effective radii are model parameters that provide the optimal fit to the data, over the observed data range. They additionally reflect real, physical half-light radii only if the models can be extrapolated to infinity.

While the introduction of additional free parameters in a fitted model will reduce the value of Δ , we show here that this is not the explanation for the improvement in the fit we obtain when changing from an $R^{1/4}$ model to an $R^{1/n}$ model.

Our profiles have at least $m = 125$ measured points. $R^{1/4}$ + exponential fits have four free parameters, i.e. $k = 4$, and Sérsic + Sérsic fits have $k = 6$. For random residuals, the expected value of Δ scales as $\sqrt{(m-k)/m}$. As a result, an improvement of only 0.8% would be expected for increasing the number of free parameters from 4 to 6. To have an improvement of 5% in Δ , a total of 16 free parameters are

needed, and for a 10% improvement, 27 free parameters are needed. For three of our light profiles an improvement of more than 10% is shown when adopting a Sérsic + Sérsic fit over an $R^{1/4}$ + exponential fit. That is, the residuals about the $R^{1/4}$ + exponential fit are not random, instead, there is structure indicating the inadequacy of this model and justifying the double Sérsic model. NGC 3551 shows little, if any, improvement in its Δ , revealing that an $R^{1/n_1} + R^{1/n_2}$ with $n_1 = 4$ and $n_2 = 1$ is appropriate for this galaxy. A summary of the values of Δ found for each type of fit applied to each of our galaxies is shown in Table 3. We do not consider NGC 6173 here since only one component is necessary to model this galaxy (see Section 3).

Unfortunately neither the ellipticity profile nor the position angle profile yielded any clues to the transition from inner to outer component. Similarly, Zibetti et al. (2005, their Fig.6) show that no change in the ellipticity profile is observed at the inflection of their surface brightness profile. In fact, there is no change in the behaviour of their ellipticity profile until ~ 160 kpc — a radius 8 times greater than their inner component's effective radius.

3 RESULTS: GALAXY SURFACE BRIGHTNESS PROFILES

GIN 478:

The obvious structure in the residual profile of Figure 3a reveals that this galaxy is not well described with a single-component $R^{1/n}$ model. Figure 3b, in which two $R^{1/n}$ models have been fitted, shows that the outer part of this galaxy's surface brightness profile is almost exponential in nature. Fitting an outer exponential (Figure 3c) shows that the profile shape of the best-fitting inner model does not change significantly, with a Sérsic index $n \sim 3$. Both of these fits have residuals of $\Delta \simeq 0.07$ mag arcsec $^{-2}$. Fitting the inner part of the profile with an $R^{1/4}$ model and the outer part of profile with an exponential (Figure 3d) increases the residuals by more than 10 per cent with $\Delta = 0.077$ mag arcsec $^{-2}$. An $R^{1/3}$ + exponential model is the optimal fit when using integer values for the Sérsic indices.

NGC 3551:

This galaxy is also not well modelled with a single $R^{1/n}$ function (Figure 4a), evidenced by the mismatch at small radii and the relatively large rms scatter Δ (c.f. Figure 4b, c and d). Figure 4b shows that the outer part of this galaxy's surface brightness profile is almost exponential in nature. Modelling the outer profile with an exponential shows that the inner $R^{1/n}$ model's profile shape does not change significantly, with a Sérsic parameter $n \sim 6$ (Figure 4c). Both of these fits have residuals of $\Delta = 0.049$ mag arcsec $^{-2}$. Figure 4d shows an $R^{1/4}$ fit to the inner component and an exponential fit to the outer component, which also has a residual of $\Delta = 0.049$ mag arcsec $^{-2}$. A Sérsic model with index $n \sim 4 - 6$ therefore appears to provide a good fit to the central galaxy in this case, with an outer exponential law again describing the envelope. The change from an

Table 2. Summary of the results of the double Sérsic model fitting, except NGC 6173 for which we present the results from the single Sérsic component fit. Column 1: galaxy name. Column 2: total absolute magnitude within a 300 kpc radius. Column 3 and 4: surface brightness μ_e at the effective radius R_e , respectively, from the inner Sérsic fit. Column 5: inner Sérsic index n_1 . Column 6: absolute magnitude within a 300 kpc radius for the inner component. Column 7 and 8: surface brightness at the effective radius, and this radius, for the outer Sérsic component. Column 9: outer Sérsic index n_2 . Column 10: absolute magnitude within a 300 kpc radius for the outer component. Given that the dominant source of error in the observed surface brightness profiles arises from uncertainties in the sky-background, all parameter errors are obtained by re-fitting the models to the images with the sky uncertainty added or subtracted.

Galaxy	M_{tot}	Inner				Outer			
	< 300 kpc	$\mu_{e,1}$ (mag arcsec $^{-2}$)	$R_{e,1}$ (arcsec)	n_1	M_{inner} < 300 kpc	$\mu_{e,2}$ (mag arcsec $^{-2}$)	$R_{e,2}$ (arcsec)	n_2	M_{outer} < 300 kpc
1	2	3	4	5	6	7	8	9	10
GIN 478	-23.03±0.45	24.08±0.13	11.5±0.9	3.0±0.1	-21.63±0.03	27.38±0.05	151.0±49.1	0.8±0.1	-22.69±0.43
NGC 3551	-22.21±0.24	26.27±0.49	86.0±18.7	6.4±0.7	-21.50±0.03	26.95±0.23	209.2±49.8	1.2±0.2	-21.40±0.22
NGC 4874	-21.78±0.09	21.44±0.23	3.8±0.3	1.1±0.2	-18.50±0.02	26.84±0.13	230.0±26.1	4.0±0.1	-21.73±0.08
NGC 6173	-22.95±3.57	30.00±5.47	788±218	14.0±7.5	–	–	–	–	–
UGC 9799	-22.26±0.45	23.17±0.17	15.7±3.1	1.4±0.2	-20.73±0.19	25.00±0.19	72.3±13.4	1.0±0.3	-21.95±0.29

Table 3. Summary of the values of Δ found for each type of fit applied to 4 of our 5 galaxies. See Section 2.2.

Galaxy	Δ (mag arcsec $^{-2}$)					
	$R^{1/n}$	$R^{1/4} + R^{1/4}$	$R^{1/3} + R^{1/3}$	$R^{1/4} + \text{Exp}$	$R^{1/n} + \text{Exp}$	$R^{1/n} + R^{1/n}$
GIN 478	0.277	0.118	0.076	0.077	0.069	0.068
NGC 3551	0.080	0.050	0.050	0.049	0.049	0.049
NGC 4874	0.053	0.042	0.046	0.057	0.054	0.040
UGC 9799	0.097	0.130	0.105	0.130	0.080	0.080

inner Sérsic parameter of $n = 4$ to $n = 6.4$ results in an increase in R_e from 37 to 86 arcsec, i.e. more than a factor of two. This is the only galaxy for which this degeneracy is seen, and this is not typical of our galaxies in general.

NGC 4874:

The residual profile in Figure 5a resembles that seen in Figures 3a and 4a, revealing additional structure that a single-component Sérsic model cannot describe. Curiously, Figure 5b shows that fitting the system with a double Sérsic model provides an outer Sérsic index of $n \sim 4$, which is not seen in any of the other galaxies. Moreover, the inner galaxy seems well characterized by a profile that is close to exponential. If we force the outer model to have an exponential profile (Figures 5c and d), the residuals increase significantly from $\Delta = 0.040$ mag arcsec $^{-2}$ to $\Delta = 0.054$ – 0.057 mag arcsec $^{-2}$. The inner component of NGC 4874 has a notably small effective radius of ~ 4 kpc. This is perhaps not unusual as Gonzalez et al. (2005) also have a number of BCGs with $R_{e,inner} < 5$ kpc.

NGC 6173:

The residual profile in Figure 6a demonstrates that a single-component fit may be adequate for this galaxy, although a large Sérsic index ($n \sim 14$) is required, and the values of μ_e and R_e are unreasonably large. Indeed, the value of $\mu_e = 30$ mag arcsec $^{-2}$ is an artificial upper limit used in the fitting code. Including an outer component decreases the residual from $\Delta = 0.077$ to $\Delta = 0.063$ (Figure

6b and 6c) and requires an inner Sérsic index of $n \sim 7$. However, given the near constant surface brightness of this outer component over the radial range for which we have data, at first glance it looks as if we failed to adequately subtract the sky background. The *additional* subtraction of the 1σ uncertainty in the sky background results in the disappearance of this near constant surface brightness component seen in Figures 6b, c and d, and the optimal fit is actually a 1-component fit, with $n = 8.7$, $R_e = 141.2$ arcsec and $\mu_e = 25.1$ mag arcsec $^{-2}$. We thus do not claim to have detected a distinct, outer halo in this system², which may therefore not be a cD galaxy. That is, this system may simply have been mis-classified as a cD galaxy because of excess flux at large radii compared to an $R^{1/4}$ model.

UGC 9799:

Figure 7b shows the double Sérsic fit to this galaxy. The inner and outer components are both modelled with $n \sim 1$, suggesting that this galaxy’s surface brightness profile may be well characterized by a double exponential. Keeping the outer component modelled with $n = 1$ (i.e. exponential) and the inner component modelled with a free value of n does not significantly change the residuals (Figure 7c) and shows that the inner component still has a Sérsic index $n \sim 1$. Not surprisingly, the affect of fitting this galaxy with a dou-

² The lack of a need for an outer component is not unprecedented. Gonzalez et al. (2000) present the light-profile for the BCG+halo in Abell 1651, and although it extends to an impressive 670 h^{-1} kpc, there is no sign of a transition radius and they show it is remarkably well fit by a single $R^{1/4}$ model.

Figure 8. HST/WFPC2 F814W images of the inner 5'' of UGC 9799. In all images north is up and east is left. *Top left:* A high contrast image showing signs of fine structure to the north-east of the nucleus of UGC 9799. *Top right:* A low contrast image showing the AGN. *Bottom left:* An unsharp-masked image, highlighting the fine structure to the north-east of the nucleus. *Bottom right:* A structure map (see Pogge & Martini 2002) highlighting the AGN.

ble exponential (not shown) does not change the residuals significantly. It is unusual though to see such a large elliptical galaxy with a low value for n , since luminous early-type galaxies usually have high Sérsic indices (Caon, Capaccioli & D'Onofrio 1993; Graham et al. 1996).

Figure 8 shows a series of I -band (F814W) HST/WFPC2 images of UGC 9799 (taken from the HST archive and observed as part of program number SNAP-8683 PI: van der Marel). Images are shown with different stretches, highlighting both low-surface brightness features (left), and the fact that this galaxy has an active nucleus (right), which is classified as Seyfert 2 in the NASA Extragalactic Database (NED). The image in the bottom left of Figure 8 is a type of residual image, created by fitting the smooth galactic starlight with elliptical isophotes and subtracting the original image from this model. Fine structure emerges using this technique. In

this case low surface brightness features to the north-east of the nucleus have been revealed. The image in the bottom right of Figure 8 is a structure map (of the kind presented by Pogge & Martini 2002) and again highlights the AGN.

For our ground-based surface brightness profiles, the inner few points (determined from the size of the relevant seeing disk) are ignored when performing the analytical fits. As a result, the bulk of the AGN contribution will also be ignored, as this will be the same size as the seeing disk. The fine structure seen in Figure 7 is also common in central cluster galaxies and can be interpreted as features, which appear as a result of the merger processes involved in the formation of cD galaxies. From a morphological point of view, UGC 9799 shows nothing that would not be expected for a cD galaxy, apart from an inner exponential fit. Although, this

was also observed in NGC 4874 and thus may be more common in cD galaxies than previously thought.

4 DISCUSSION

Constraining the surface brightness profiles of the faint envelopes in cD galaxies is important for constraining current models of cD galaxy formation and cluster dynamics. There is evidence from the globular cluster population, and the near-infrared galaxy luminosity function, to suggest that BCGs experienced their mergers long ago (Jordan et al. 2004; Ellis & Jones 2004), yet the presence of (un-erased) tidal streams (e.g. Gregg & West 1998; Trentham & Mobasher 1998) would appear to favour a more recent formation epoch. One of the earliest studies of the low surface brightness haloes of cD galaxies was performed by Carter (1977), who found that the total luminosity did not converge even at a radius of 300 kpc. This was later confirmed by Lugger (1984), who additionally found that a de Vaucouleurs $R^{1/4}$ model consistently underestimated the surface brightness profiles of cD galaxies at large radii (see also Schombert 1986). These observations have been confirmed in recent years by deep imaging of central cluster galaxies (e.g. Feldmeier et al. 2002, 2004a, b; Lin & Mohr 2004; Adami et al. 2005; Gonzalez, Zabludoff & Zaritsky 2005; Kemp et al. 2005; Krick, Bernstein & Pimblet 2006; Liu et al. 2005; Mihos et al. 2005; Zibetti et al. 2005) which clearly indicate the presence of an extended stellar envelope, albeit relative to an inner $R^{1/4}$ component. The need for two Sérsic components, rather than one, is clearly illustrated in Gonzalez, Zabludoff & Zaritsky (2003, their Figs. 1 & 2). Furthermore, it has also been shown that the Petrosian properties of central cluster galaxies display distinct properties, which can be interpreted as an indicator of cD galaxy haloes, independent of an assumed $R^{1/4}$ light-profile for the central galaxy (Brough et al. 2005; Patel et al. 2006).

We note that our photometry alone does not indicate whether the outer ‘component’ is physically distinguished from the inner ‘component’. In general, however, a *single* Sérsic function provides a good fit to ordinary elliptical galaxies, with little or no structure in their resultant residual profiles. The structure seen in the residual profiles for 4 of our 5 cD galaxies is reminiscent of that seen when fitting a single Sérsic function to a spiral galaxy, and is suggestive of two distinct components. The failure of a single Sérsic function to match the observed stellar distribution is physical evidence that four of our objects are different from ordinary elliptical galaxies, but we caution that they may still be single physical entities.

A small fraction of the ICL, and thus envelopes around cD galaxies, probably originates from stars which have been gravitationally ejected by supermassive black hole binaries at the centres of elliptical galaxies within the cluster (e.g. Holly-Bockelmann et al. 2006). Recently, Graham (2004) has shown that the central stellar mass deficit in “core” galaxies — thought to have formed in “dry” mergers — is roughly 0.1 per cent of their total stellar mass (see also Ferrarese et al. 2006). This mass deficit is roughly equal to the (combined) mass of the central black hole in ellipticals, and is also consistent with theoretical predictions on the orbital decay of binary black holes (Ebisuzaki, Makino & Okumura

1991; Milosavljević & Merritt 2001). Most recently, in high-precision, N -body simulations, Merritt (2006) has shown that virtually all of the mass deficit is generated during the rapid, initial phases of binary formation, not after the binary becomes hard. He obtains mass deficits on the order of the mass of the binary’s larger black hole, and so one can expect the intracluster light (from this mechanism) to roughly equal ~ 0.1 per cent of the cluster light in spheroids³.

Observations of multiple nuclei within brightest cluster galaxies (e.g. Hoessel & Schneider 1985; Postman & Lauer 1995; Seigar, Lynam & Chorney 2003) and low surface brightness tidal features (e.g. van Dokkum 2005) are considered strong evidence that massive galaxies are growing at the centres of rich clusters by accreting their less massive neighbours (Hausman & Ostriker 1978). Such merger events are also thought to be partly responsible for the formation of extended (low surface brightness) envelopes and intracluster light (Ostriker & Tremaine 1975; Ostriker & Hausman 1977; Hill & Oegerle 1998; Moore et al. 1996; Muccione & Ciotti 2004; Willman et al. 2004). This is demonstrated in recent semi-analytical models (e.g., Purcell, Bullock & Zentner 2007) and N -body simulations (e.g., Conroy, Wechsler & Kravtsov 2007). Moreover, close galaxy-galaxy encounters can strip stars from deep within their potential well. These stars may then be liberated by the overall cluster tidal field (Merritt 1984; Moore et al. 1996), to become what is known as the intracluster light (ICL: Zwicky 1951; Welch & Sastry 1971; Oemler 1973; Thuan & Kormendy 1977). Furthermore, the large numbers of ultra compact dwarf galaxies found in galaxy clusters suggests that this process may be rather efficient (e.g., Bekki et al. 2003; Côté 2005; Drinkwater et al. 2005; Gnedin 2003; Mieske, Hilker & Infante 2005). It is also likely responsible for the existence of intracluster: planetary nebulae (Arnaboldi et al. 2004; Aguerra et al. 2005a; Feldmeier et al. 2004b; Gerhard et al. 2005); red giant stars (Ferguson, Tanvir & von Hippel 1998; Durrell et al. 2002); novae (Neill, Shara & Oegerle 2005); and supernova (Gal-Yam et al. 2003).

Our results reveal, given the validity of these processes, that they result (in three instances) in an exponential-like distribution of stars around the central dominant galaxy. More precisely, for three of our five galaxies, an inner Sérsic model plus an outer exponential model provides a good fit to the data. In one galaxy, NGC 6173, no outer exponential model is required, and in NGC 4874, the outer light profile is best described with an $R^{1/4}$ model rather than an exponential model.

If the envelopes associated with cD galaxies trace a surrounding dark matter halo, then one might expect them to be described by a Sérsic function with n around 2.5 to 3. This is because hierarchical Λ CDM simulations produce a near universal profile shape for dark matter halos on all scales, the projection of which is well described by a Sérsic $R^{1/n}$ model with $n \sim 3$ (Łokas & Mamon 2001; Merritt et al. 2005, 2006).

Curiously, N -body simulations of cold collapses (and disk galaxy mergers) also result in haloes (and merger rem-

³ This is an upper estimate because in gas rich mergers, gas facilitates the decay of the binary black hole, and consequently less stars are ejected.

nants) having, in projection, $R^{1/3}$ -like profiles (e.g., Willman et al. 2004, their Fig.7; Aceves, Velaquez & Cruz 2006; Merritt et al. 2006). Interestingly, a closer inspection of old data (e.g. Figures 4–6 in van Albada 1982) reveals obvious and systematic deviations from the $R^{1/4}$ model in the sense that an $R^{1/n}$ model with $n < 4$ provides a better fit to the data presented there. If the halo or intracluster light around cD galaxies traces the dominant dark matter potential, one does not expect this envelope to be described with an $R^{1/4}$ model. Of course, baryonic processes may well result in a different stellar distribution to the dark matter distribution, and studies suggest this can lead to a flattening of the inner density profile (Nipoti et al. 2004), which is effectively equivalent to a reduction in the Sérsic index.

Demarco et al. (2003) have analysed the distribution of X-ray gas in a sample of 24 real galaxy clusters. They found it was well described by a Sérsic function having values $0.8 < n < 2.3$. With the exception of NGC 4874, this range is in good agreement with the values reported here for the outer component of our cD galaxies, and suggests that this envelope is indeed tracing the (azimuthally-averaged) intracluster light. Moreover, our exponential-like outer profiles match the exponential ICL profile in Abell 3888 (Krick et al. 2006). When more observations become available, it will be interesting to see whether the distribution of the intracluster stellar probes, such as planetary nebula and globular clusters, follow an exponential or an $R^{1/4}$ radial distribution. It will also be interesting to know if the intragroup light (e.g., Da Rocha & de Oliveira 2005; Faltenbacher & Mathews 2005; White et al. 2003) behaves in a similar or different manner.

The mean BCG+ICL light-profile obtained from the stacked cluster image reported in Zibetti et al. (2005) is plotted using a *linear* radial axis in Zibetti & White (2004, their Fig. 1)⁴. One can immediately see by eyeball examination that the outer light-profile is well approximated by an exponential (i.e., a straight line in that figure). This is in good agreement with our independent data and the (cluster halo) X-ray data from Demarco et al. (2003), but at odds with the $R^{1/4}$ model used in Gonzalez et al. (2005), and at odds with a projected NFW model. We do however note that the shape of the ICL profile in Zibetti et al. (2005) is different, suggestive of a Sérsic index greater than 1. This difference arose from their new corrections for mask incompleteness and their new method of determining the sky background. The latter involved simultaneously fitting an NFW model for the ICL and some constant value for the sky background level. The problem with such an approach is that the fitted constant effectively modifies the real ICL profile to produce (as best as it can) an NFW profile, even when the real ICL may not have such a form. Fitting an $R^{1/4}$ model from 150 to 500 kpc, Zibetti et al. (2005, their section 5.1) report an effective radius R_e of 250–300 kpc for the ICL, somewhat larger than the values we observe in our sample (Table 4).

4.1 Relative contribution of the stellar envelope to the total luminosity of cD galaxies

We use the analytical fits from Table 2 to determine the relative contribution of the stellar envelope to the total luminosity of the galaxy plus envelope, i.e. the envelope-to-total ratio. We compute two estimates of this flux ratio. One of these, $(E/T)_{300}$, comes from truncating the models at a radius of 300 kpc, as done in Gonzalez et al. (2005). Our second estimate assumes no truncation, and is denoted $(E/T)_{\text{tot}}$. Due to the extended nature of the envelope, our $(E/T)_{\text{tot}}$ values are somewhat different when compared to our $(E/T)_{300}$ values, although only by ~ 10 per cent at most. Both quantities are listed in Table 4. It should be noted that since the radial extent of our surface brightness profiles is ~ 100 kpc, although 223 kpc for GIN 478, that we have to extrapolate to estimate both the $(E/T)_{300}$ and $(E/T)_{\text{tot}}$ values.

In most cases the extended stellar envelope contributes around 60 to 80 per cent of the total R -band luminosity when no truncation radius is applied and the models are extrapolated to infinity. When the profiles are truncated at 300 kpc, the envelope contributes between ~ 45 to 80 per cent. The exception is NGC 4874 (the only galaxy with an $R^{1/4}$ envelope) which has $E/T \simeq 95$ –98 per cent. These flux ratios lie in the same range found by Gonzalez et al. (2005), who reported E/T ratios of around 0.9 but as low as 0.4 (their Figure 7). However, Zibetti et al. (2005) find a slightly lower value. They find that the ICL contributes 10.9 per cent to the total cluster light and the central galaxy contributes 21.9 per cent. This is equivalent to an E/T ratio of ~ 33 per cent. However, taking into account the errors in the measurements, E/T ratios in the range 25 to 45 per cent are allowed. The high end of their range is therefore consistent with the results found here.

For the three cDs best described with an $R^{1/n}$ galaxy plus exponential envelope, the galaxy-to-envelope size ratio (given by the ratio of the effective radii $R_{e,1}/R_{e,2}$) ranges from ~ 0.1 to ~ 0.4 . In contrast, using double $R^{1/4}$ models, Gonzalez et al. (2005) report ratios of ~ 0.1 down to ~ 0.025 , i.e. envelopes 10 to 40 times larger in size than the inner component. One of our remaining two galaxies appears to have no distinct envelope, and the other has an $R^{1/4}$ envelope 60 times greater in size than the central galaxy.

5 SUMMARY

We have observed 5 cD galaxies to a depth of $\mu_R = 26.5$ mag arcsec⁻², and we have determined the shapes of the surface brightness profile of their outer stellar envelopes.

The results of previous attempts to model the intracluster light or extended stellar envelope suggested that a universal model applies. For example, Gonzalez et al. (2005) report that both the central part of the cD and the intracluster light are both well described by an $R^{1/4}$ surface brightness model. In general, previous studies of this kind have only tried fitting a surface brightness model of one kind. Our approach of fitting a Sérsic model to the extended halo provides a means to actually measure, rather than pre-ordain the actual stellar distribution, albeit within the confines of the Sérsic model.

⁴ Zibetti & White (2004) use 654 clusters, while Zibetti et al. (2005) use 683.

Table 4. Results using the double Sérsic model to derive ratios of physical parameters. Column 1: galaxy name. Column 2: effective radius of the central galaxy. Column 3: effective radius of the ICL or envelope. Column 4: galaxy-to-envelope size ratio, given by the ratio of the effective radii $R_{e,1}/R_{e,2}$. Column 5 and 6: envelope-to-total ratio calculated by extrapolating the profiles to infinity, $(E/T)_{\text{tot}}$, and 300 kpc, $(E/T)_{300}$.

Galaxy	$R_{e,1}$ (kpc)	$R_{e,2}$ (kpc)	$R_{e,1}/R_{e,2}$	$(E/T)_{\text{tot}}$	$(E/T)_{300}$
1	2	3	4	5	6
GIN 478	19.9±1.6	261.2±84.9	0.076±0.019	0.82±0.13	0.73±0.13
NGC 3551	53.3±11.6	129.7±30.9	0.411±0.072	0.59±0.04	0.47±0.05
NGC 4874	1.8±0.1	108.1±12.3	0.017±0.002	0.98±0.01	0.95±0.01
NGC 6173	1073.1±296.8	–	–	–	–
UGC 9799	10.5±2.0	48.4±9.0	0.217±0.042	0.77±0.14	0.76±0.14

Our analysis suggests that the surface brightness profiles of cD galaxies (including their envelopes) are best modelled by a double Sérsic function. While an inner $R^{1/4}$ model is sufficient for some cDs, we have found that the inner Sérsic index can vary significantly from object to object (from $n \sim 1$ to $n \sim 7$). An outer exponential model seems appropriate for three of our four, 2-component systems. One galaxy (NGC 4874) appears to have an $R^{1/4}$ envelope. Typically, when present, the envelope contributes around 60 to 90 per cent of the total (galaxy + ICL) light, and the galaxy-to-envelope size ratio is ~ 0.1 to ~ 0.4 .

ACKNOWLEDGMENTS

The Jacobus Kapteyn Telescope (JKT) was operated on the island of La Palma by the Isaac Newton Group in the Spanish Observatorio del Roque de los Muchachos of the Instituto de Astrofísica de Canarias. This research has made use of the NASA/IPAC Extragalactic Database (NED) which is operated by the Jet Propulsion Laboratory, California Institute of Technology, under contract with the National Aeronautics and Space Administration. This work made use of observations made with the NASA/ESA Hubble Space Telescope, obtained from the data archive at the Space Telescope Science Institute. STScI is operated by the Association of Universities for Research in Astronomy, Inc. under NASA contract NAS 5-26555. MSS acknowledges partial support from a Gary McCue Fellowship through the Center for Cosmology at UC Irvine. The authors wish to thank Paul Lynam for useful comments and suggestions. The authors also would like to thank the referee, Dr. S. Zibetti, for useful suggestions and comments.

REFERENCES

- Abell G. O., 1958, *ApJS*, 3, 211
Aceves H., Velaquez H., Cruz F., 2006, *MNRAS*, 373, 632
Adami C., Slezak E., Durret F., Conselice C. J., Cuillandre J. C., Gallagher J. S., Mazure A., Pelló R., Picat, J. P., Ulmer M. P., 2005, *A&A*, 429, 39
Aguerri J. A. L., Gerhard O., Arnaboldi M., Napolitano N. R., Castro-Rodriguez N., Freeman K. C., 2005a, *AJ*, 129, 2585
Aguerri J. A. L., Elias-Rosa N., Corsini E. M., Muñoz-Tuñón C., 2005b, *A&A*, 434, 109
Andredakis Y. C., Peletier R. F., Balcells M., 1995, *MNRAS*, 275, 874
Arnaboldi M., Gerhard O., Aguerri J. A. L., Freeman K. C., Napolitano N. R., Okamura S., Yasuda N., 2004, *ApJ*, 614, L33
Balcells M., Graham A. W., Domínguez-Palmero L., Peletier R. F., 2003, *ApJ*, 582, L79
Barazza F. D., Binggeli B., Jerjen H., 2002, *A&A*, 391, 823
Barth A. J., 2007, *AJ*, 133, 1085
Bautz L. P., Morgan W. W., 1970, *ApJ*, 162, L149
Bekki K., Couch W. J., Drinkwater M. J., Shioya Y., 2003, *MNRAS*, 344, 399
Brough S., Collins C. A., Burke D. J., Lynam P. D., Mann R. G., 2005, *MNRAS*, 364, 1354
Caon N., Capaccioli M., D’Onofrio M., 1993, *MNRAS*, 265, 1013
Carter D., 1977, *MNRAS*, 178, 137
Conroy C., Wechsler R. H., Kravtsov A. V., 2007, *ApJ*, submitted (astro-ph/0703374)
Côté P., 2005, in *Near-fields cosmology with dwarf elliptical galaxies*, IAU Colloquium Proceedings 198, eds Jerjen H., Binggeli B. (Cambridge: Cambridge University Press, p 269
da Rocha C., de Oliveira C.M., 2005, *MNRAS*, 364, 1069
Dalcanton J. J., Hogan C. J., 2001, *ApJ*, 561, 35
de Jong, R. S., 1996, *A&AS*, 118, 557
de Vaucouleurs G., 1948, *AnAp*, 11, 247
Demarco, R., Magnard, F., Durret, F., & Márquez, I. 2003, *A&A*, 407, 437
Dressler A., 1984, *ApJ*, 281, 512
Drinkwater M. J., Evstigneeva E., Gregg M. D., Jones J. B., Phillipps S., Jurek R., 2005, in *Near-fields cosmology with dwarf elliptical galaxies*, IAU Colloquium Proceedings 198, eds Jerjen H., Binggeli B. (Cambridge: Cambridge University Press, p 398
Durrell P. R., Ciardullo R., Feldmeier J. J., Jacoby G. H., Sigurdsson S., 2002, *ApJ*, 570, 119
Ebisuzaki T., Makino J., Okumura S.K., 1991, *Nature*, 354, 212
Einasto J., 1965, *Trudy Inst. Astrofiz. Alma-Ata*, 5, 87
Ellis S. C., Jones, L. R., 2004, *MNRAS*, 348, 165
Faltenbacher A., Mathews W.G., 2005, *MNRAS*, 362, 498
Feldmeier, J. J., Mihos J. C., Morrison H. L., Rodney S. A., Harding P., 2002, *ApJ*, 575, 779
Feldmeier J. J., Mihos J. C., Morrison H. L., Harding P., Kaib N., Dubinski J., 2004a, *ApJ*, 609, 617
Feldmeier J. J., Ciardullo R., Jacoby G. H., Durrell P. R., 2004b, *ApJ*, 615, 196

- Ferguson H. C., Tanvir N. R., von Hippel T., 1998, *Nature*, 391, 461
- Ferrarese L. et al., 2006, *ApJS*, 164, 334
- Gal-Yam A., Maoz D., Guhathakurta P., Filippenko, A. V., 2003, *AJ*, 125, 1087
- Gerhard O., Arnaboldi M., Freeman K. C., Kashikawa N., Okamura S., Yasuda N., 2005, *ApJ*, 621, L93
- Gnedin O. Y., 2003, *ApJ*, 589, 752
- Gonzalez A. H., Zabludoff A. I., Zaritsky D., Dalcanton J. I., 2000, *ApJ*, 536, 561
- Gonzalez A. H., Zabludoff A. I., Zaritsky D., 2003, *Ap&SS*, 285, 67
- Gonzalez A. H., Zabludoff A. I., Zaritsky D., 2005, *ApJ*, 618, 195
- Graham A., Lauer T. R., Colless M., Postman M., 1996, *ApJ*, 465, 534
- Graham, A. W., 2002, *ApJ*, 568, L13
- Graham A. W., Guzmán R., 2003, *AJ*, 125, 2936
- Graham A. W., Erwin P., Trujillo I., Asensio-Ramos A., 2003, *AJ*, 125, 2951
- Graham A. W., 2004, *ApJ*, 613, L33
- Graham A. W., Driver S. P., 2005, *PASA*, 22, 118
- Gregg M. D., West, M. J., 1998, *Nature*, 396, 549
- Hausman M. A., Ostriker J. P., 1978, *ApJ*, 224, 320
- Hill, J. M., Oegerle W. R., 1993, *AJ*, 106, 831
- Hill J. M., Oegerle W. R., 1998, *AJ*, 116, 1529
- Hoessel J. G., Schneider D. P., 1985, *AJ*, 90, 1648
- Holley-Bockelmann K., Sigurdsson S., Mihos J. C., Feldmeier J. J., Ciardullo, R. McBride C., 2006, *ApJL*, submitted [astro-ph/0512344]
- Jedrzejewski R. I., 1987, *MNRAS*, 226, 747
- Jerjen H., Kalnajs A., Binggeli B., 2000, *A&A*, 358, 845
- Jordán A., Côté P., West M. J., Marzke R. O., Minniti D., Rejkuba M., 2004, *AJ*, 127, 24
- Kahaner D., Moler C., Nash S., 1989, Englewood Cliffs: Prentice Hall, 1989
- Kemp S. N., de la Fuente E., Franco-Balderas A., Meabrun J., 2005, *ApJ*, 624, 680
- Kormendy J., Djorgovski S., 1989, *ARA&A*, 27, 235
- Krick J. E., Bernstein R. A., Pimbblet K. A., 2006, *AJ*, 131, 168
- Laine S., van der Marel R. P., Lauer T. R., Postman M., O'Dea C. P., Owen F. N., 2003, *AJ*, 125, 478
- Landolt A. U., 1992, *AJ*, 104, 340
- Lauer T. R., Postman M., 1992, *ApJ*, 400, L47
- Lauer T. R. et al., 1995, *AJ*, 110, 2622
- Lauer T. R., Postman M., 1994, *ApJ*, 425, 418
- Lin Y.-T., Mohr J. J., 2004, *ApJ*, 617, 879
- Liu Y., Zhou X., Ma J., Wu H., Yang Y., Li J., Chen J., 2005, *AJ*, 129, 2628
- Lokas E. L., Mamon G. A., 2001, *MNRAS*, 321, 155
- Lugger P. M., 1984, *ApJ*, 286, 106
- Merritt D., 1984, *ApJ*, 276, 26
- Merritt D., Navarro J. F., Ludlow A., Jenkins A., 2005, *ApJ*, 624, L85
- Merritt D., 2006, *ApJ*, 648, 976
- Merritt D., Graham A. W., Moore B., Diemand J., Terzić B., 2006, *AJ*, 132, 2685
- Mieske S., Hilker M., Infante L., 2005, in *Near-fields cosmology with dwarf elliptical galaxies*, IAU Colloquium Proceedings 198, eds Jerjen H., Binggeli B. (Cambridge: Cambridge University Press), p 404
- Mihos J. C., Harding P., Feldmeier J., Morrison H., 2005, *ApJ*, 631, L41
- Milosavljević M., Merritt D., 2001, *ApJ*, 563, 34
- Moore B., Katz N., Lake G., Dressler A., Oemler A., 1996, *Nature*, 379, 613
- Muccione V., Ciotti L., 2004, *A&A*, 421, 58
- Navarro J. F., Frenk C. S., White S. D. M., 1996, *ApJ*, 462, 563 [NFW]
- Neill J. D., Shara, M. M., Oegerle W. R., 2005, *ApJ*, 618, 692
- Nipoti C., Treu T., Ciotti L., Stiavelli M., 2004, *MNRAS*, 355, 1119
- Oegerle W. R., Hill J. M., 2001, *AJ*, 122, 2858
- Oemler A., 1973, *ApJ*, 180, 11
- Ostriker J. P., Hausman M. A., 1977, *ApJ*, 217, L125
- Ostriker J. P., Tremaine S. D., 1975, *ApJ*, 202, L113
- Patel P., Maddox S., Pearce F. R., Aragón-Salamanca A., Conway E., 2006, *MNRAS*, 370, 851
- Pogge R. W., Martini P., 2002, *ApJ*, 569, 624
- Postman M., Lauer T. R., 1995, *ApJ*, 440, 28
- Press W. H., Flannery B. P., Teukolsky S. A., Vetterling W. T., 1986, in *Galactic Astronomy* (Cambridge: Cambridge Univ. Press), p 176
- Pritchet, C., Kline, M. I. 1981, *AJ*, 86, 1859
- Prugniel Ph., Simien F., 1997, *A&A*, 321, 111
- Purcell C. W., Bullock, J. S., Zentner A. R., 2007, *ApJ*, submitted (astro-ph/0703004)
- Schombert J., 1986, *ApJS*, 60, 603
- Schomber J. M., Bothun G. D., 1987, *AJ*, 93, 60
- Seigar M. S., James P. A., 1998, *MNRAS*, 299, 672
- Seigar M. S., Lynam P. D., Chorney N. E., 2003, *MNRAS*, 344, 110
- Sérsic, J.-L. 1963, *Boletín de la Asociación Argentina de Astronomía*, vol.6, p.41
- Sérsic, J.-L., 1968, *Atlas de Galaxias Australes* (Cordoba: Obs. Astron.)
- Thuan T. X., Kormendy J., 1977, *PASP*, 89, 466
- Trentham N., Mobasher B., 1998, *MNRAS*, 293, 53
- Trujillo I., Erwin P., Asensio Ramos A., Graham A. W., 2004, *AJ*, 127, 1917
- van Albada T. S., 1982, *MNRAS*, 201, 939
- van Dokkum, P. G., 2005, *AJ*, 130, 2647
- Welch G. A., Sastry G. N., 1971, *ApJ*, 169, L3
- White P. M., Bothun G., Guerrero M. A., West M. J., Barkhouse W. A., 2003, *ApJ*, 585, 739
- Willman B., Governato F., Wadsley J., Quinn T., 2004, *MNRAS*, 355, 159
- Worthey G., 1994, *ApJS*, 95, 107
- Young C. K., Currie, M. J., 1994, *MNRAS*, 273, 1141
- Zibetti S., White S. D. M., 2004, in *Outskirts of Galaxy Clusters: Life in the Suburbs*, IAU Colloquium 195, ed. A. Diaferio, p 226
- Zibetti S., White S. D. M., Schneider D. P., Brinkmann J., 2005, *MNRAS*, 358, 949
- Zwicky, F. 1951, *PASP*, 63, 61

This figure "seigar_fig2.jpg" is available in "jpg" format from:

<http://arxiv.org/ps/astro-ph/0612229v2>

This figure "seigar_fig8a.jpg" is available in "jpg" format from:

<http://arxiv.org/ps/astro-ph/0612229v2>

This figure "seigar_fig8b.jpg" is available in "jpg" format from:

<http://arxiv.org/ps/astro-ph/0612229v2>

This figure "seigar_fig8c.jpg" is available in "jpg" format from:

<http://arxiv.org/ps/astro-ph/0612229v2>

This figure "seigar_fig8d.jpg" is available in "jpg" format from:

<http://arxiv.org/ps/astro-ph/0612229v2>